mathematics

MDPI

Article

Simulation Analysis of Dynamic Damage Probability Modelling for Laser Systems

Jiaowei Shi [1], Shiyan Sun [1,*], Jun Xie [1] and Chaobing Zheng [2]

[1] Weapon Engineering College, Naval University of Engineering, Wuhan 430034, China; 21100705@nue.edu.cn (J.S.); hwanze21cn@sina.com (J.X.)
[2] School of Information Science and Engineering, Wuhan University of Science and Technology, Wuhan 430081, China; zhengchaobing@wust.edu.cn
* Correspondence: 0909061028@nue.edu.cn

Abstract: The paper proposes a method that analyses the dynamic damage probability of laser systems to address the shortcomings of the quantitative model for the damage probability of laser systems. Firstly, the far-field energy density distribution model is constructed according to the power spectrum inversion method. Then, the instantaneous on-target spot power density distribution is equivalently portrayed based on the combination of the far-field power density and the missile target characteristics. Next, the instantaneous on-target spot is combined with the tracking and aiming error to obtain the probability distribution of the energy density of the long-period on-target spot. Finally, the temperature probability distribution is obtained by analyzing the relation between the target energy density and the temperature of the inner wall of the warhead. Consequently, the damage probability was calculated. The simulation shows that there is a unique maximum damage probability when the target is flying in a straight line and the laser system strikes the missile sideways. The method can provide support for the shooting timing of high-energy laser systems.

Keywords: on-target power density; on-target energy density; tracking and aiming error; dynamic damage probability

MSC: 65C05; 78-10

Citation: Shi, J.; Sun, S.; Xie, J.; Zheng, C. Simulation Analysis of Dynamic Damage Probability Modelling for Laser Systems. *Mathematics* **2023**, *11*, 4097. https://doi.org/10.3390/math11194097

Academic Editor: Paolo Mercorelli

Received: 20 August 2023
Revised: 18 September 2023
Accepted: 24 September 2023
Published: 27 September 2023

1. Introduction

Anti-ship missiles are weapons used to attack surface ships, which can be launched by submarines from underwater as well as by surface ships or aircraft. They are equipped with high manoeuvrability, flying fast at a low height. The missile attack course is generally divided into an initial section, a self-control section, and a self-guided section [1,2]. The self-guided segment begins when the missile is more than 10 km from the target and ends when it reaches the target. As an end-of-line defence weapon, the self-guided section of the missile is the main section of the high-energy laser system that intercepts the target [3,4]. In addition, the damage probability of a weapon, as a key indicator for operational decision-making, is of great significance. Therefore, this paper mainly researches the probability of destruction in the self-guided segment of a missile target.

At present, there are few references that directly discuss the damage probability of laser weapons. However, the elements involved in the damage probability include laser atmospheric transmission, tracking and aiming errors, and laser–target interaction. This paper conducts research based on the above elements. In [5], the authors established a laser weapon power density model based on the analysis of the transmission characteristics of the laser in the atmosphere and the tracking errors. In [6], the authors take the effects of atmospheric transmissions and the far-field spot area of the laser system into consideration, simulating the effectiveness of a 10,000-watt high-energy laser system by calculating the atmospheric transmittance [7,8], the quality of the laser beam after being affected by

atmospheric turbulence [9–15], the spot area of the target in the far field, the power density of the target in the far field [16–20], and the cumulative energy density [21,22], which gives the optimal intercept radius and the damage probability of the 10,000-watt high-energy laser system in different atmospheric environments. In [23], the authors proposed a systematic averaging method from the physical mechanism of the formation of the long-period averaged power intensity distribution, modelling the long-period averaged power intensity distribution under the effect of tracking and aiming errors and beam drift. According to the different characteristics of the capture link and the tracking link, they deduced the closed expression of the long-period averaged power intensity distribution under tracking and aiming errors [24–26]. According to [27], continuous wave (CW) laser-induced nanowelding holds great promise for micro and nano devices. However, the heat effect from CW laser irradiation may harm the manufactured devices because of the lengthy irradiation duration. The simulation results show that an increase in irradiation duration will slightly improve the welding temperature but greatly expand the heat-affected area when the irradiation time exceeds 100 ms. In [28], the authors build a three-dimensional physical model of continuous laser-irradiated material according to the actual situation of continuous laser-heated target material. Combined with the actual boundary conditions, the analytical expression of the transient temperature field of the material is derived based on integral transformation. In [29], under the condition that the tracking error of the system is a homogeneous square derivable, each state is experienced in a zero-mean normal process. The authors derived the equation for the dynamic damage probability level of a high-energy laser system by means of clear physical concepts and rigorous mathematical deduction. In [30], the authors define the damage probability of a high-energy laser system under the conditions of successful target capture and conduct an analysis. The authors do not combine specific target characteristics to analyse the damage probability in detail in [29,30]; although the authors combine target characteristics, the model granularity is large and the results are not accurate enough in [5,6]. In [23], the authors determine the average spot intensity distribution under the effect of turbulence and tracking and aiming errors, but they do not provide the form of the probability distribution of spot intensity, which is not conducive to the subsequent modelling of the damage probability. In other references, the authors analysed the atmospheric transmission effect of lasers, as well as the description of the tracking and aiming errors and laser-target interactions, but did not systematically discuss the damage probability for a specific target. In the paper, we start from the definition of damage probability and analyse the concept of target damage and the origin of probability in the kill chain. What's more, we analyse and model each link of the kill chain to obtain the final damage probability model.

The next section of this paper is set up as follows: In Section 2, the definition of the damage probability of the high-energy laser system is analysed. In Section 3, firstly, the instantaneous on-target power density of the high-energy laser system is derived, and the probability distribution of on-target energy density is obtained by combining the tracking and aiming errors. Then, the probability distribution of the temperature in the inner wall of the combatant shell is provided according to the probability distribution of the on-target energy density. The computational model of the dynamic damage probability is given according to the probability distribution of the temperature in the inner wall of the combatant shell. In Section 4, the dynamic damage probability is simulated and analysed with specific examples. In Section 5, a conclusion and outlook of the damage probability of high-energy laser system are provided.

2. Definition of the Damage Probability of a Laser System

The mechanism by which high-energy laser systems damage targets is not the same as that of traditional weapons systems. Thus, it is necessary to redefine the damage probability of high-energy laser systems in terms of damage. The operational target is designed to finish a certain task; thus, the target damage is not equal to the disappearance of the target, but the loss of target operating function, which can prevent completion of the intended

task. Quantitative characterization of damage is required to build the model. At present, there are three main ways to characterise damage. First, the laser parameters are directly selected as the damage characterization quantity. Second, the target function parameters are selected as the damage characterization quantity. Third, the intermediate parameters of the target damage process are selected as the damage edge characterization quantity. The third damage characterization method combines the advantages of the first two, so the third characterization method is selected to characterise the damage of the warhead. In other words, the temperature of the inner wall of the warhead is used as the target damage characterization quantity. After the damage characterization is extracted, it is necessary to set the damage criterion and carry out the damage assessment. Combining the above damage assessment processes and analyzing the probability sources in the process, the damage probability model can be built.

When a traditional weapon system fires at a target, hitting and damaging the target is a common event, so the probability of damaging the target is equal to the probability of hitting the target and the conditional probability of damaging the target. Because the high-energy laser system requires sustained fire to damage, it is not enough to characterise the damage capability of a high-energy laser system by hit probability; thus, the damage capability needs to be discussed based on the probability density of tracking and aiming errors. At present, there is no clear definition of the damage probability of high-energy laser systems, so this paper starts from the principle of laser damage to the target. For the damage of the missile warhead, the damage probability is defined as the probability that the internal temperature of the warhead is greater than the internal temperature threshold of the target warhead when the laser irradiates the warhead.

In the actual combat process, there is a random error in the temperature rise of the inner wall of the shell of the warhead caused by irradiation by the high-energy laser system. Random errors mainly include on-target energy density distribution errors. On-target energy density probability distribution is mainly embodied in the probability distribution of the tracking and aiming errors. According to the definition of the damage probability and the random distribution characteristics of the temperature of the inner wall of the shell of the warhead, the damage probability schematic can be illustrated as shown Figure 1. In the figure, T_D denotes the temperature threshold of the inner wall of the warhead when the target is damaged. T_1, T_2 denote the inner wall temperature produced by continuous laser irradiation of the target. When the laser dwell time is short, the temperature of the inner wall of the shell is relatively low, and only the tail, with its high temperature, exceeds the target damage temperature threshold, meaning the probability of damage, P_{kill}, will be relatively low. When the dwell time is long, the temperature of the inner wall of the shell is much higher, and thus the damage probability will be close to 1.

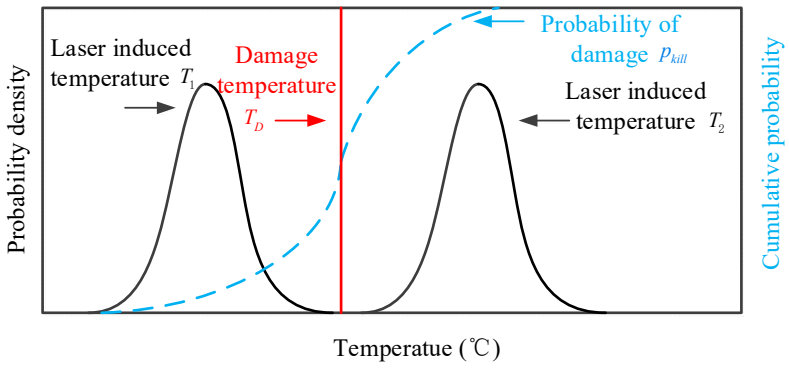

Figure 1. Schematic diagram of damage probability of laser weapons.

According to the above analysis, the target is not damaged when the temperature of the inner wall of warhead is less than T_D; on the contrary, when the temperature of the

inner wall of warhead is greater than T_D, the target is regarded as damaged, and then the damage probability model can be defined as:

$$P_{kill} = \int_{T_D}^{\infty} f(T)dT \quad (1)$$

3. Damage Probability Model

The construction of the laser damage probability model is mainly embodied in the construction of the probability distribution model of the on-target energy density and conversion between the energy density and the temperature of the inner wall of the warhead. The on-target energy density can be regarded as a number of instantaneous on-target spot superpositions in space, and the probability distribution of the position of each instantaneous on-target spot will be consistent with the probability distribution of tracking and aiming errors, meaning its probability mainly comes from the randomness of tracking and aiming errors. After the construction of the on-target energy density model, the probability distribution of the on-target energy density can be converted into the probability distribution of the temperature of the inner wall of the warhead through temperature field analysis; then, the target damage probability can be achieved through damage assessment. The process of constructing the damage probability model is shown in Figure 2. The subsequent content is mainly divided into the construction of instantaneous on-target energy density distribution models. The construction of on-target energy density probability distribution models is based on the tracking and aiming errors and damage assessment analysis.

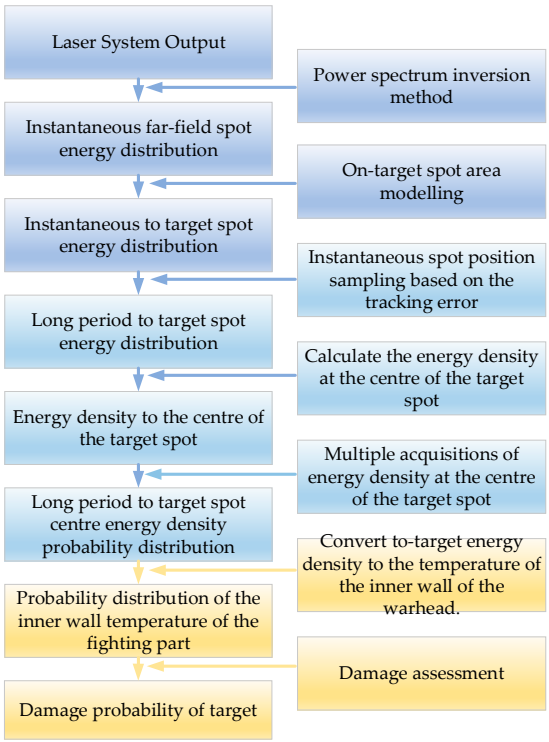

Figure 2. Flowchart for construction of the damage probability model.

3.1. Instantaneous On-Target Energy Distribution

Generally speaking, the time of instantaneous spots refers to less than 0.05 s. In that time, it can be approximated that the on-target power density remains unchanged, which can degrade the relation between the instantaneous on-target energy and the instantaneous on-target spot power from an integral in time to a product with time. There are two factors

involved in the instantaneous on-target spot power distribution, the first of which is the far-field power distribution. The on-target power is mainly affected by the laser-atmosphere absorption effect and the atmospheric turbulence effect, which can be obtained through the atmospheric transmittance and the phase screen technique. The second factor is the on-target spot area, which is affected by the beam expansion angle and the curvature of the target surface and can be obtained using the Monte Carlo method.

The instantaneous on-target spot energy density distribution is irregular and random, so the core problem of instantaneous on-target energy density distribution inscription is how to carry out the equivalent simplification. The basis of the equivalent simplification is construction of a far-field spot energy density distribution model and an on-target spot area model. The far-field spot energy density distribution can be calculated according to the atmospheric turbulence inversion method. At present, the on-target spot area is generally represented by the far-field spot area, and the schematic diagram of the far-field spot and on-target spot is shown in Figure 3. The shaded part of Figure 3 denotes the cross-sectional spot of the laser beam, while the on-target spot area is the intersection area of the laser beam and the target. Generally, the on-target spot area is larger than the far-field spot area, and if the far-field spot is used instead of the on-target spot to calculate the on-target power density, the on-target power density will be overestimated. Therefore, firstly, we need to calculate the on-target spot area. Then, the on-target energy density distribution is equivalently inscribed on the on-target spot area. In order to facilitate the discrete analysis of the on-target energy density distribution, the on-target energy density distribution is generally equivalent to the on-target energy density distribution within the effective spot radius.

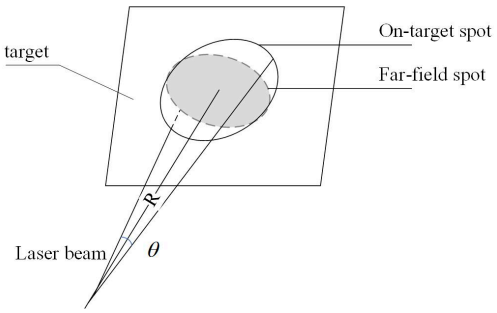

Figure 3. Schematic diagram of a far-field spot and on-target spot.

3.1.1. Far-Field Spot Distribution

When the emitted laser is a Gaussian beam, the light intensity distribution in the cross-section of an ideal Gaussian beam is:

$$I(x, y) = I_0 \exp(-\frac{2(x^2 + y^2)}{w^2}) \quad (2)$$

where I_0 denotes central peak light intensity and w denotes beam waist. When the Gaussian beam is transmitted in atmospheric turbulence, it is only meaningful to study the effect of atmospheric turbulence on lasers statistically, since atmospheric turbulence is random. Assuming that atmospheric turbulence is a simple statistical model, a common approach is to treat the turbulence as a finite number of phase screens. Currently, a common method for constructing a phase screen is to use a turbulent refractive index spectrum, and a complex Gaussian random number matrix to generate a phase space complex random field and then derive the spatial distribution of the two-dimensional phase by an inverse Fourier transform. This method is called power spectrum inversion. The far-field spot energy density distribution can be obtained by simulating the turbulent phase screen according to the power spectrum inversion method. The specific calculation process of the power spectrum inversion method is as follows.

Assuming that atmospheric turbulence is isotropic and locally homogeneous, a refractive index spectral density function can be obtained based on the Kolmogonov atmospheric refractive index structure function, which describes the fluctuations in the refractive index due to atmospheric turbulence. This function was later optimised by Van-Karman, who gave a more accurate description of the refractive index fluctuations. The Van-Karman atmospheric refractive index spectral density function is as follows:

$$\Phi_n(\kappa, z) = 0.033 C_n^2(z)(\kappa_0^2 + \kappa^2)^{-11/6} \exp(\kappa/\kappa_m) \tag{3}$$

where κ is the number of waves in 3D space and the range of values of κ is $\kappa_0 < \kappa < \kappa_m$; $\kappa_0 = 2\pi/L_0$, $\kappa_m = 5.92/l_0$, l_0, and L_0 denote the inner and outer scales of turbulence, respectively; z denotes the laser propagation distance; and C_n^2 denotes the turbulence structure constant. The atmospheric phase power spectrum, $\Phi_\phi(\kappa_x, \kappa_y, \kappa_z, z)$, can be expressed as a function of the atmospheric refractive index spectrum, $\Phi_n(\kappa_x, \kappa_y, \kappa_z, z)$. When the laser is transmitted, there is a relationship between the atmospheric power spectrum $\Phi_\phi(\kappa_x, \kappa_y)$ and the atmospheric refractive index spectrum $\Phi_n(\kappa_x, \kappa_y)$ in the perpendicular section of the transmission direction, which is shown in the following equation.

$$\Phi_\phi(\kappa_x, \kappa_y) = 2\pi k^2 \Delta z \Phi_n(\kappa_x, \kappa_y) \tag{4}$$

Here, Δz denotes the thickness of the turbulence which the laser is transmitted through ($k = 2\pi/\lambda$). Firstly, the Gaussian random matrix is filtered with $\Phi_\phi(\kappa_x, \kappa_y)$; secondly, the atmospheric phase screen function is obtained by taking the Fourier transform of the filtered Gaussian random matrix, as shown in Equation (5).

$$\phi_{sh}(x, y) = \mathrm{C} \sum_{p=1}^{N_p} \sum_{m=0}^{N_x} \sum_{n=0}^{N_y} R(\kappa_x, \kappa_y) F_\phi(\kappa_x, \kappa_y) \exp(2\pi i(\frac{x}{3^p D_x} + \frac{y}{3^p D_y})) \tag{5}$$

Here, $\phi_{sh}(x, y)$ denotes the atmospheric phase screen function; (x, y) represents airspace coordinates; Δx and Δy denote the airspace sampling interval; m and n denote intervals; (κ_x, κ_y) denotes the frequency domain coordinates; $\Delta\kappa_x$ and $\Delta\kappa_y$ denote the frequency domain sampling interval; $m\prime$ and $n\prime$ are intervals; the constant, C, is derived from the scale factor, $(\Delta\kappa_x \Delta\kappa_y)^{1/2}$; and $R(k_x, k_y)$ denotes a random number that follows a Gaussian distribution, $r \sim N(0, 1)$.

According to the phase screen derived from the power spectrum inversion method, the representation of the far-field spot power density distribution, $I_{yc}(x, y)$, is shown in Equation (6) and the schematic diagram of the energy density distribution is shown in Figure 4.

$$I_{yc}(x, y) = (ifft2(H(f_x, f_y) * fft2(I(x, y) \exp(i\phi_{sh}(x, y)))))2 \tag{6}$$

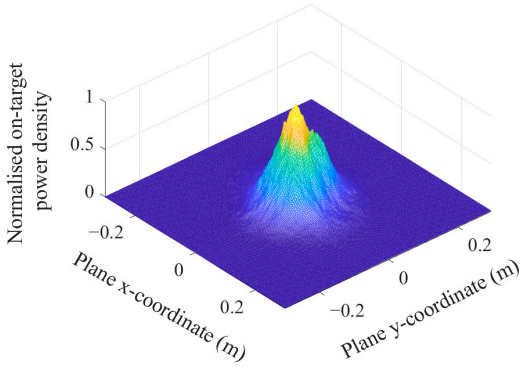

Figure 4. Far-field spot distribution.

Here, $fft2$, $fft2$ denote the forward and the inverse Fourier transforms, respectively. $H(f_x, f_y)$ denotes the transfer function for free-space diffraction and $\phi_{sh}(x, y)$ denotes the phase screen function.

3.1.2. Calculating On-Target Spot Area Based on Monte Carlo

The on-target spot area is closely related to the shape of the target surface. The information on the shape of the target surface cannot be accurately obtained during combat, meaning it is necessary to carry out appropriate equivalence for the target combat component, as shown in Figure 5. Then, the angle between the launching direction of the laser system and the flight direction of the missile, as well as the radius of the target to calculate the on-target spot area, are calculated as shown in Equation (7).

$$A = f(r, \alpha, r_t) \tag{7}$$

(**a**) (**b**)

Figure 5. Simplified diagram of the strike combat element of a high-energy laser system. (**a**) Schematic diagram of the strike fighting unit. (**b**) Simplified diagram of a strike force warhead.

Here, A denotes the laser system on-target spot area, r denotes the far-field spot radius of the laser system, α denotes the angle between the launching direction of the laser system and the flight direction of the missile, and r_t denotes the radius of the warhead.

According to the simplified diagram of the striking warhead, it can be seen that the laser beam can be approximated as a cone and the warhead can be equated to a cylinder. The intersection area of them can be calculated by the Monte Carlo method. The process of solving it is as follows:

Assuming that our ship takes the vertical direction as the z-axis and the bow direction as the Y-axis, a three-dimensional coordinate system (XYZ) with the ship as the origin is established. Assuming that half of the far-field dispersion angle of the laser system is θ_0, then the relation between the radius, r, of the cross-section and the height, z, is as shown in Equation (8). The mathematical model of laser ballistic theory is shown in Equation (9).

$$\tan\theta_0 = r/z \approx \theta_0 \tag{8}$$

$$x^2 + y^2 = (z\theta_0)^2 \tag{9}$$

Assume that the coordinates of the target in the ship's coordinate system are (x_t, y_t, z_t). The coordinates of the vulnerable parts of the target in the ship's coordinate system are (x_{ys}, y_{ys}, z_{ys}). Using these, the mathematical model of the laser beam pointing at the vulnerable area can be calculated. The mathematical model of the laser beam needs to be tilted along the azimuth angle, ϕ, and pitch angles, φ, a process that can be viewed as a transformation of the coordinate system. Firstly the cone is rotated anti-clockwise along

the z-axis, $\pi/2 - \varphi$. The cone is then rotated anti-clockwise along the z-axis, ϕ. Then, the mathematical model of the laser beam can be obtained as shown in the following equation.

$$(x_1, y_1, z_1, 1) = (x0, y0, z0, 1) \begin{bmatrix} 1 & 0 & 0 & 0 \\ 0 & \sin\varphi & -\cos\varphi & 0 \\ 0 & \cos\varphi & \sin\varphi & 0 \\ 0 & 0 & 0 & 1 \end{bmatrix} \begin{bmatrix} \cos\phi & -\sin\phi & 0 & 0 \\ \sin\phi & \cos\phi & 0 & 0 \\ 0 & 0 & 1 & 0 \\ 0 & 0 & 0 & 1 \end{bmatrix} \tag{10}$$

Here, $(x0, y0, z0)$ denotes the coordinate points on the original unrotated laser beam and $(x1, y1, z1)$ denotes the coordinate point on the light path towards a vulnerable part of the target. In order to simplify the calculation, the attitude of the missile in this paper takes the horizontal state. If the body of the missile target is equivalent to a cylinder, then the missile body mathematical model is:

$$\begin{cases} x_2 = x \quad x_t - \frac{l}{2} \le x \le x_t + \frac{l}{2} \\ y_2 = r\sin\gamma + y_t \\ z_2 = -r\cos\gamma + z_t \end{cases} \tag{11}$$

where r denotes the radius of the missile body, which is a known constant and is taken as r = k. γ is the angle between the polar diameter and the z-axis. The joint Equations (10) and (11) provide a mathematical model of the spot area where the laser trajectory intersects the target projectile. It is not easy to find the analytical solution of the above model, so the Monte Carlo method can be used to find the numerical solution of the on-target spot area directly. The key flow of the solution is as follows.

➢ Cylindrical Surface Uniform Drop Strategy

Dropping uniformly on a cylindrical surface requires ensuring that the probability densities are equal at any point on the cylinder. Since x and y, z in the probability density function are independent of each other, they can be defined as shown in Equation (12).

$$f(x_0, y_0, z_0) = f(x_0) f(y_0, z_0) \tag{12}$$

Here, $f(x_0)$ and $f(y_0, z_0)$ denote the probability density functions at $x = x_0$, (y_0, z_0), respectively. To make it equal everywhere, it is sufficient to make the drop point obey a uniform distribution on the x interval of the cylinder. The probability density of the drop point on the circumference of the cylinder must be equal everywhere. The probability density function that is equal everywhere on the circumference of the circle is shown in Equation (13), which is converted to a probability density function on the angle as in Equation (14).

$$f(y_0, z_0) = \frac{1}{2\pi r} \tag{13}$$

$$f(\theta) = \frac{1}{2\pi} \tag{14}$$

Here, r denotes the radius of the circle. Thus, the rule for randomly taking the drop point is as follows:

The x-coordinates of the points are taken uniformly on the x-axis, while the y-coordinates and z-coordinates of the points are taken uniformly based on polar coordinates. N angles, θ, are generated uniformly in $0 - 2\pi$; then, according to the transformation relation of polar coordinates to x–y coordinates, as shown in Equation (15), the random data of y, z can be obtained.

$$\begin{cases} z = rcos\theta \\ y = rsin\theta \end{cases} \tag{15}$$

➢ Strategies for Determining Where the Drop Point is Inside the Cone

After points are dropped, it is necessary to determine whether the drop point is inside the cone. As show in Figure 6, according to the characteristics of the cone, the problem can

be converted to determine the angle between the vector $\overrightarrow{OP}$ formed by the drop point and the origin and the vector $\overrightarrow{OO'}$. If the angle, $\angle\left(\overrightarrow{OP}, \overrightarrow{OO'}\right)$, is less than the half angle of the cone, then it is inside, otherwise it is outside.

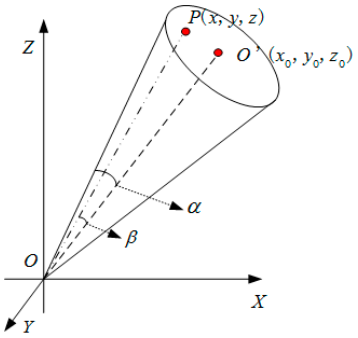

Figure 6. Schematic diagram for determining whether the drop point is inside the cone.

The number of points that fall inside the cone is $N_{\text{in\_cone}}$, while number of all points is N. Since there will be two intersecting surfaces of coherence between the cone and the cylinder, the area of the first intersecting surfaces is given in Equation (16).

$$S_{\text{db}} = \frac{N_{\text{in\_cone}}}{N}\pi rl \tag{16}$$

Here, r denotes the radius of cylinder and l denotes the length of the cylinder.

3.1.3. On-Target Spot Distribution

The energy density distribution of the far-field spot is regarded as the distribution on the plane, and the actual distribution on the target should is regarded as the distribution of the spatial surface. The direction of laser emission is not necessarily perpendicular to the target surface, so the actual distribution area of the target surface spot is larger than the area of the far-field spot. In order to facilitate the analysis, the on-target spot area can be equivalent to the plane of the circle. The principle of equivalence is as follows: ① The shape of the far-field spot of the target energy density distribution doesn't change, only the overall zoom on-target power density value. ② The area of the intersecting surface is equal to the area of the plane circle. ③ On-target power and the corresponding far-field power are equal, as shown in Equation (17). After the equivalence, the far-field spot energy density distribution map and on-target energy density distribution map are as shown in Figure 7.

$$\iint\limits_{S_{\text{yc}}} I_{\text{yc}}(x,y)dxdy = \iint\limits_{S_{\text{db}}} I_{\text{db}}(x,y)dxdy \tag{17}$$

Here, $I_{yc}(x,y)$ and $I_{db}(x,y)$ denote the far-field and on-target energy density distribution functions, while S_{yc} and S_{db} denote the effective spot areas of the far-field spot and the on-target spot, respectively.

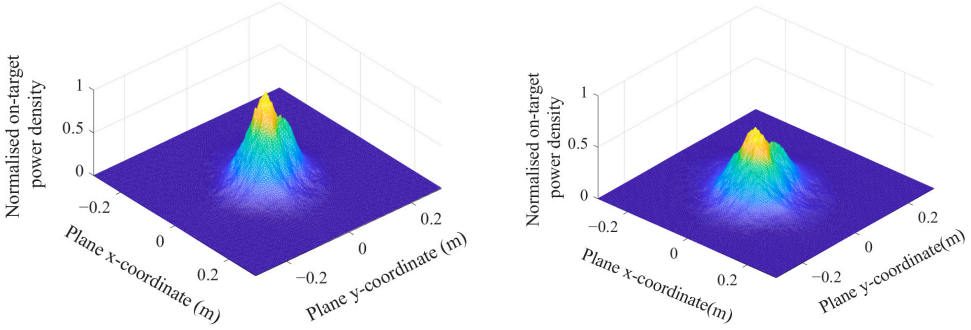

(**a**) (**b**)

Figure 7. Simplified distribution of on-target spot power density. (**a**) Far-field spot distribution. (**b**) On-target Spot Distribution.

3.1.4. Calculation of Spot Centre and Effective Spot Radius

The spot centre refers to the position of the centre of the energy density distribution of the spot using the power density as the weight. The effective spot is defined as the circular domain taking the spot centre point as the centre, which accounts for 84% of the total power, as shown in Figure 8. The process of calculating the spot centre of mass and effective spot radius is as follows:

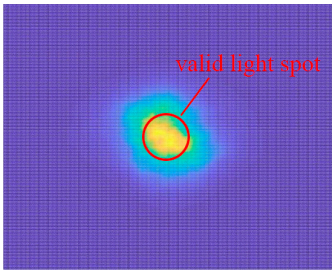

Figure 8. Effective spot schematic.

Setting a position, z, along the direction of laser emission, the measurement yields a transverse energy density distribution, $I(x, y)$, of the beam. The centre of the spot is equal to the first order moment of the energy density distribution, as shown in the following equation.

$$\begin{cases} \overline{x} = \frac{\int\int xI(x,y)dxdy}{\int\int I(x,y)dxdy} \\ \overline{y} = \frac{\int\int yI(x,y)dxdy}{\int\int I(x,y)dxdy} \end{cases} \tag{18}$$

Here, (x, y) denotes the position of a point on the spot. After taking out the centre of the spot, the effective radius of the spot is calculated as follows:

① Based on the centre point of the spot, the radius is equal to the minimum distance between the centre point and the boundary of the receiving screen, as shown in Equation (19).

$$r = \min(x_{\text{center}}, W - x_{\text{center}}, y_{\text{center}}, H - y_{\text{center}}) \tag{19}$$

Here, r denotes radius, $(x_{\text{center}}, y_{\text{center}})$ denotes the centre point of the spot, and W and H denote the width and height of the receiving screen, respectively.

② The data corresponding to the circular outer rectangle of the radius is taken out and the cumulative intensity and the percentage of energy in the whole receiving screen is calculated as shown in Equation (20).

$$\eta = \frac{\sum\limits_{(x,y)\in\Omega} I(x,y)}{\sum\limits_{(x,y)\in S} I(x,y)} \tag{20}$$

③ If $\eta \geq 84\%$, $r = r - 1$, calculate the energy share of the next outer rectangle, η_{next}, according to ②. If $\eta_{\text{next}} \leq 84\%$, then the spot should traverse all points within the outer rectangle, which is a circle of the radius, r. If the distance between the current point and the centre point is less than the radius, it is considered as a point within the spot; if it is greater than the radius, it is not considered.

④ Cycle ② and ③ to calculate the effective spot radius. The above process to find the effective spot is shown in Figure 8.

3.2. On-Target Energy Density Distribution Based on Tracking and Aiming Errors

3.2.1. Probability Density Distribution of Tracking and Aiming Errors

Currently there are no unified definitions of tracking and aiming errors, so this paper adopts the definitions in [31]. The tracking error is defined as the deviation between the instrument's visual axis and the target's line of sight. The aiming error is defined as the average value of the deviation between the instrument view axis and the target view axis. The sources of tracking errors include sensor error, dynamic hysteresis error, torque error, and other kinds of perturbation errors; the sources of targeting errors include the parallax between the tracking axis and the main axis, the error caused by the deformation of the axial system or structure, the error caused by atmospheric refraction, the deviation between the measurement point and the tracking point, etc. It is difficult to completely decouple the various error sources and analyse them individually to achieve a theoretical study. Therefore, the probability density distribution due to random errors is generally obtained through experimental statistics.

The tracking error of laser systems is discussed in relation to the concept of shoot error in conventional weapons, where the continuous laser is discretised according to time. In traditional weapons, aiming error refers to the deviation between the scattering centre and the target centre, and the scattering error is worth the deviation between the blow-up point and the scattering centre. In the laser system, the aiming error refers to the deviation between the instantaneous spot intensity integration centre and the target aiming point, while the tracking error refers to the deviation between the instantaneous spot and the spot intensity integration centre. Therefore, the tracking and aiming error of the laser system can be borrowed from the concept of the firing error of traditional artillery shells, the aiming error can be used to characterise the accuracy of the discrete spot, and the tracking error can be used to characterise the denseness of the discrete spot.

Under the same firing elements, the aiming error can be approximated as a constant value, expressed as:

$$\hat{\varphi}(x_c, z_c) = (u_x, u_z) \tag{21}$$

where (u_x, u_z) denotes the deviation of the centre of integration of the on-target spot from the aiming point.

The probability density distribution of the tracking error is denoted as:

$$\hat{\varphi}(x_s, z_s) = \frac{\rho^2}{\pi B_d B_f} \exp\left[-\rho^2\left(\frac{x_s^2}{B_d^2} + \frac{z_s^2}{B_f^2}\right)\right] \tag{22}$$

where ρ denotes a normal constant, which takes the value 0.4769 generally. The intermediate tracking errors are B_d and B_f. According to the definition of probabilistic error, it can be seen that, assuming that the on-target spot approximately obeys a two-dimensional Gaussian

distribution ($B_d = B_f = 0.6745\sigma$L), σ is the tracking mean square error of the high-energy laser system.

The height angle error, z, and azimuth angle error, x, of laser shooting are:

$$z = z_c + z_s,\ x = x_c + x_s \tag{23}$$

The median error in elevation and median error, E_x, in the azimuth of the shot are:

$$E_x = B_d,\ E_z = B_f \tag{24}$$

Assuming that the principal semiaxes of the aiming error ellipse and the tracking error ellipse coincide, the density of the distribution of the tracking and aiming errors has the standard form shown in Equation (25).

$$\hat{\varphi}(x,z) = \frac{\rho^2}{\pi E_x E_z} \exp\left[-\rho^2\left(\frac{(x-u_x)^2}{E_x^2} + \frac{(z-u_z)^2}{E_z^2}\right)\right] \tag{25}$$

3.2.2. Spot Centre Energy Density Based on Tracking Errors

Through the instantaneous spot characteristics combined with the probability distribution of the tracking and aiming errors of the laser system, an analytical equation for the spot energy distribution of the long period can be obtained as shown in Equation (26) and schematically figured as shown in Figure 9b.

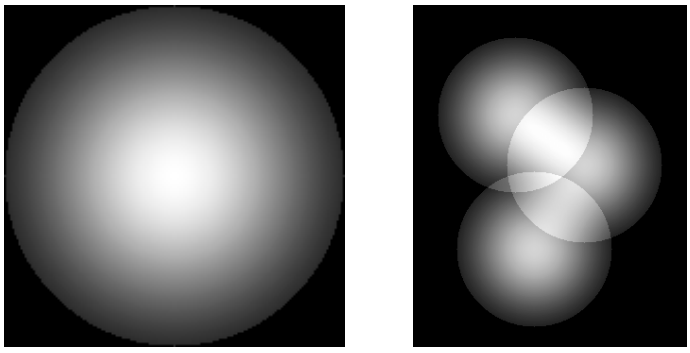

(**a**) (**b**)

Figure 9. Schematic diagram of the energy density of the target. (**a**) Distribution of energy density of a single instantaneous spot. (**b**) Spot energy density distribution based on following errors.

In the above figures, Figure 9a denotes the instantaneous spot energy density distribution, while Figure 9b indicates instantaneous spot positions that are randomly distributed according to the tracking and aiming errors, with three instantaneous random spots spatially superimposed. The computational model of Figure 9b is shown in Equation (26).

$$E_{\text{inc}}(x,y) = \sum_{k=1}^{N} I_k(\hat{\varphi}(x,y))\Delta t \tag{26}$$

Here, $E_{\text{inc}}(x,y)$ denotes on-target energy density distribution, $I_k(x,y)$ denotes the kth instantaneous spot distribution, $I_{db}(x,y)$, k = 1,2,...N. $\hat{\varphi}$(x, y) denotes the instantaneous spot location (x,y), which obeys the tracking and aiming probability distribution, $\hat{\varphi}$. Δt denotes the duration of continuous laser irradiation.

The calculation process of on-target energy density probability distribution is as follows: Firstly, the spot centre of the long-period spot energy density distribution is determined, which is analogous to the determination of the instantaneous spot centre; Secondly, the combination instantaneous spot centre with a spot radius is to determine the average on-target energy density; Thirdly, a number of simulations are used to obtain a

multiplied average on-target energy density and statistical histograms are drawn; Finally, the probability distribution function can be obtained according to the statistical histograms.

3.3. Missile Warhead Damage Assessment Analysis

The principle of battle damage is to heat the inner wall of the shell, resulting in an explosion. Therefore, it is necessary to convert the on-target energy density to the temperature of the inner wall of the shell and then analyse the damage by comparing it with the temperature threshold of the inner wall of the target shell. Assuming a thin shell wall of $\delta < \mathrm{R}/50$ and an absorption depth of no more than δ, the heat generated by the inner wall of the shell is negligible. Assuming that the shell wall material is in the solid phase and is isotropic, the energy balance equation for the heated part is as shown in Equation (27).

$$\frac{1}{\kappa}\frac{\partial T}{\partial t} = \frac{\partial^2 T}{\partial x^2} + \frac{\partial^2 T}{\partial y^2} + \frac{\partial^2 T}{\partial z^2} \tag{27}$$

Here, T denotes the wall temperature of the combat shell, t denotes time, and $\kappa = k/\rho c$ denotes the "effective" or average heat diffusion coefficient of the outer wall of the combatant, which is a constant value, where k is the thermal conductivity, ρ denotes density, and c denotes specific heat.

Assuming that x_{edge} and y_{edge} denote half of the length to the x-direction or y-direction of the target spot, respectively, when both satisfy:

$$\frac{2\sqrt{\kappa\tau_{\mathrm{p}}}}{x_{\mathrm{edge}}} \leq 0.2,\ \frac{2\sqrt{\kappa\tau_{\mathrm{p}}}}{y_{\mathrm{edge}}} \leq 0.2 \tag{28}$$

where τ_{p} denotes the laser irradiation time, then the laser can be considered to be one-dimensional in the z-direction. Consequently, the formula simplifies to:

$$\frac{1}{\kappa}\frac{\partial T}{\partial t} - \frac{\partial^2 T}{\partial z^2} = 0 \tag{29}$$

The laser continuously irradiates the cylinder shell. Thus, the heat conduction problem is one with an external heat source, which derives its heat from the average on-target power of the laser irradiating the point. The inner surface can be considered as an adiabatic edge.

$$\begin{aligned} \mathrm{T}(x,y,z,0) &= \mathrm{T}_0 \\ -k\frac{\partial T}{\partial z}\bigg|_{z=0} &= \mathrm{A}E_{\mathrm{inc}}/t \\ k\frac{\partial T}{\partial z}\bigg|_{z=\delta} &= 0 \end{aligned} \tag{30}$$

Here, A denotes the absorption of laser light by the target, E_{inc} denotes the on-target energy density, and t denotes the laser irradiation time. δ denotes shell thickness, and the inner surface is considered as an insulated edge.

The solution to Equation (30) is:

$$\begin{aligned} T(x,y,z,t) = T_0 + \tfrac{AE_{inc}}{t}\Bigg\{ \tfrac{\kappa t}{k\delta} + \tfrac{\delta}{k}\left[\tfrac{3(\delta-z)^2-\delta^2}{6\delta^2}\right] - \\ \tfrac{2\delta}{\pi^2 k}\sum_{n=1}^{\infty}\tfrac{(-1)^n}{n^2}\exp\left(\tfrac{-k\pi^2 n^2 t}{\delta^2}\right)\cos\left[\tfrac{n\pi(\delta-z)}{\delta}\right]\Bigg\} \end{aligned} \tag{31}$$

Through Equation (31), we can obtain the temperature of the inner wall of the combat shell, so as to compare with the inner wall temperature threshold of the combat part explosion and judge whether the target is damaged or not. Combining the on-target energy density probability distribution and Equation (31) leads to a temperature probability distribution. Moreover, damage probability can be calculated according to Equation (1).

4. Simulation Analysis

Assuming the subject is an interceptor missile targeting a certain type of anti-ship missile, the high-energy laser system, target characteristics, and environmental characteristics are assumed as follows:

High-energy laser system characteristics: 300kW high-energy laser system with a full power single stabilised emission time of 10 s. The transmittance of the laser emission system is $K_s = 0.7$. Assuming that the tracking mean square error, σ, of the laser system is 10 μrad, the mean value, u, is 8 μrad. The intermediate errors of the tracking error are $B_d = 0.6745\sigma L$ and $B_f = 0.6745\sigma$L.

Target characteristics: a flight speed of Mach 0.9; a 20 m cruising altitude straight to the target ship; a target radius of 0.8 m and length of 3 m. The damage temperature threshold of the inner wall of the shell is 480 degrees Celsius.

Environmental characteristics: an atmospheric transmission attenuation coefficient of 0.05% and atmospheric coherence length of 4.69 cm.

Because of the relatively large amount of calculation involved in damage probability, damage probability is calculated at every interval delta_t in the target flight time. In this paper, we take the full-power single-shot full-time output of the laser system and regard the damage probability as successful interception when it is greater than 90%. Under the condition of high visibility, the effective range of the laser system to strike the warhead is 5 km, and the schematic diagram of the laser system to intercept the invading missile is as shown in Figure 10. Missile M is approaching Ship P in a straight line, and the effective range of laser system O is 0.2 km–5 km, as shown in Figure 10. When M enters effective range, the position of target M is (4582.5, 2000, 20) and the position of ship P is (2000, 2000, 0). When the target is at a distance of 5 km, according to Equation (9), the far-field spot area can be calculated as 81.91 cm^2. The far-field spot energy density distribution is shown in Figure 11a. The on-target spot area is 102.47 cm^2 and the on-target energy density distribution is shown in Figure 11b. The probability distribution of the tracking and aiming error of the laser system is $\hat{\varphi}(x,z) = 63.7\exp\left[-200\left((x-0.04)^2+(z-0.04)^2\right)\right]$, as shown in Figure 11c. At a sustained strike of 10 s, the on-target spot energy density distribution formed is as shown in Figure 11d. The energy density of the centre of the target spot is 1246 J/cm^2. With 100 simulations, a mean-to-target energy density probability distribution can be obtained, as shown in Figure 11. According to Equation (31), the probability density distribution of the temperature of the inner wall of the fighting part at this time is shown in Figure 11b, and the parameter settings of Equation (31) are shown in Table 1.

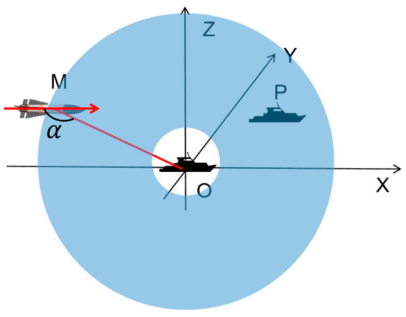

Figure 10. Schematic diagram of a laser system for anti-missile defence.

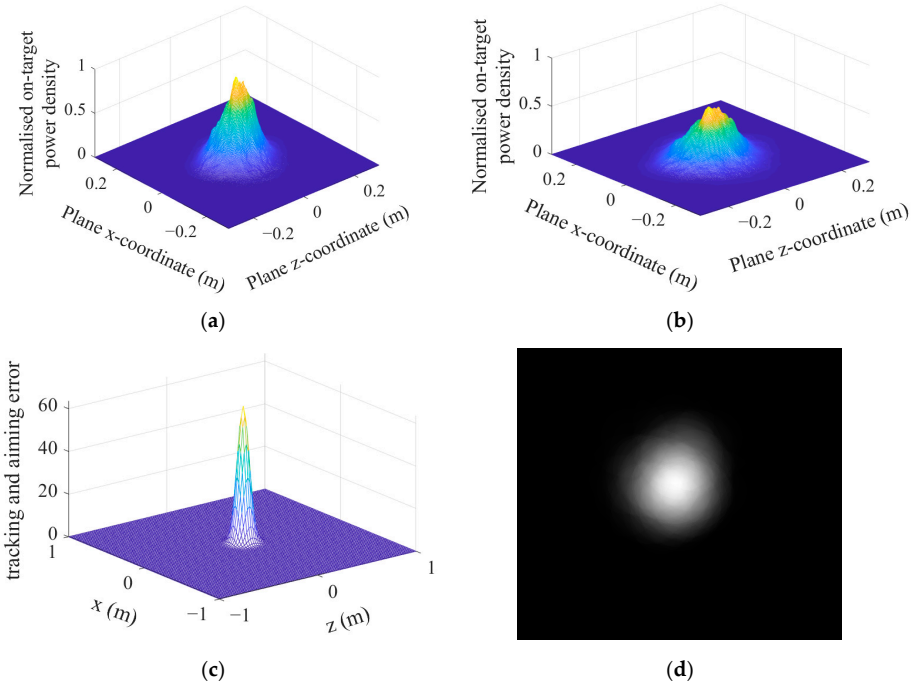

Figure 11. Schematic of on-target energy density inference. (**a**) Far-field spot energy density 3D surface. (**b**) On-target spot energy density 3D surface. (**c**) Probability distribution curve of tracking error. (**d**) Schematic diagram of spot distribution based on probabilistic sampling of tracking error.

Table 1. Parameter table for the heat transfer equation.

Performance Parameters	δ [cm]	ρ [g/cm^3]	k [W/(cm·K)]	c [J/(g·K)]	A	T_0 [°C]	θ [°]
2024-T3AL	0.5	2.77	1.73	1	0.112	20	90

According to Equation (31), it can be seen that there is a linear relationship between the temperature of the inner wall of the combat shell and the energy density of the centre of the on-target spot, meaning their curve trends remain basically the same. The red line in Figure 12b denotes the temperature damage threshold of the target's warhead. Since the temperature of the inner wall is much smaller than the temperature threshold, combined with Equation (1), the probability of the battle section's damage can be calculated to be 0 percent; that is, the probability of the target's damage is 0 percent.

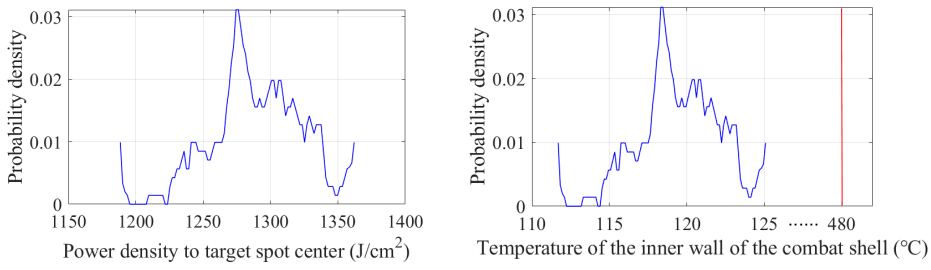

Figure 12. Plot of energy density at the centre of the target spot versus the temperature of the inner wall of the combatant housing. (**a**) Power density probability distribution at the centre of the target spot. (**b**) Temperature probability distribution of the inner wall of the combat housing.

Combined with the full path of the target, the damage probability curve for the full path within the effective range is as shown in Figure 13. The data of the damage probability

curve is shown in Table 2. In Table 2, Ft denotes the target flight time and Pd denotes the damage probability.

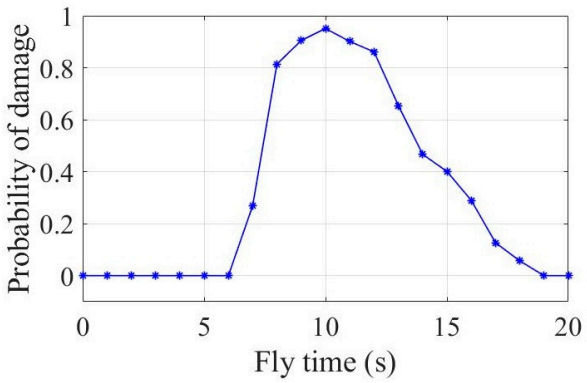

Figure 13. All-route damage probability curves.

Table 2. All-route damage probability table.

Ft(s)	0∣6	7	8	9	10	11	12	13	14	15	16	17	18	19 ∣ 20
Pd	0	0.27	0.81	0.91	0.95	0.90	0.86	0.65	0.47	0.40	0.29	0.13	0.06	0

According to Figure 9 and Table 2, it can be seen that the damage probability becomes higher and higher over 0–10 s, increasing to a peak value of 95% in 10 s and then gradually decreasing over 10–20 s before finally decreasing to almost 0. Therefore, when the target is flying for 10 s, the target is 3522.5 m from the protected ship, the damage probability of laser system is the highest, and it is also the best time to shoot for the laser system.

5. Conclusions

This paper chiefly studies the following aspects. Firstly, the damage probability of the laser system is defined and the rough model is analysed. Secondly, the far-field spot energy density distribution model is constructed through the power spectrum inversion method. Moreover, the instantaneous on-target spot energy density distribution is simplified equivalently for a specific target. Accordingly, the simplified spot centre of gravity and the effective spot radius are quantitatively computed. Thirdly, the probability distribution function for obtaining the follow-up error is analysed. The long period on-target spot energy density is also combined with the tracking error to obtain the probability distribution function and is analysed to obtain the tracking error. The equivalent instantaneous spot and tracking error are combined in order to obtain the probability distribution of the long-period on-target spot centre energy density. Finally, the temperature field is analysed through the temperature field of the on-target energy density caused by the temperature change in the inner wall of the combatant shell. This can be used to judge whether the target is destroyed or not, so as to convert the probability distribution of the on-target energy density to the damage probability, given that the analysis framework of dynamic damage probability in this paper can provide effective support for the shooting timing of laser systems.

The granularity of the model is not specific enough. In order to make the damage probability characterization value more accurate, the next step can be improved as follows: ① The on-target energy density model should be an integral model of multiple instantaneous spots in space-time. Subsequently, a continuous model of the instantaneous on-target spot energy density distribution can be constructed over time and then combined with the multiple integral model, which can be solved by using the Monte Carlo method and the number theory grid method. ② The tracking and aiming errors are not only related

to the laser system, but also related to the flight speed of the target, the image quality of photoelectric capture, etc. Therefore, in order to improve the credibility of the damage probability, the mechanism model of the tracking and aiming errors will be constructed to reduce the granularity of the model in the future.

Author Contributions: Conceptualization, J.S. and S.S.; methodology, J.S. and S.S.; validation, J.X. and C.Z.; writing—original draft preparation, J.S.; writing—reviewing and editing, J.X. and C.Z. All authors have read and agreed to the published version of the manuscript.

Funding: This work was supported in part by Fundamental Strengthening Programme Technical Area Fund Grant 2019-JCJQ-J-J-049.

Institutional Review Board Statement: Not applicable.

Informed Consent Statement: Not applicable.

Data Availability Statement: Not applicable.

Acknowledgments: The authors would like to thank for Z.S. for the excellent technical support and X.W. for critically reviewing the manuscript.

Conflicts of Interest: The authors declare no conflict of interest.

References

1. Li, Y.; Wang, M.Y.; Zhang, J. Damaging evaluation of high-energy laser weapon to ballistic missile. *Infrared Laser Eng.* **2006**, *35*, 588–592.
2. Paul, M. Laser weapon prepares to zap enemy missiles. *New Sci.* **2008**, *200*, 26–27.
3. Lavan, M. High Energy Laser Systems for Short Range Defense. *Acta Phys. Pol.* **2009**, *115*, 959–963. [CrossRef]
4. Liu, J.R.; Du, T.J.; Wang, L.J. *High Energy Laser System Test and Evaluation*; National Defence Industry Press: Beijing, China, 2014.
5. Xu, D.X. Modeling and Simulation on Damage Ability of Shipborne Laser Weapon. *Syst. Simul. Technol.* **2021**, *17*, 94–97.
6. Xu, C.R.; Sun, S.Y.; She, B.; Zhou, J.F. Research on Combat Effectiveness of Ten-Kilowatt Shipborne Laser Weapon Against UAV. *J. Ordnance Equip. Eng.* **2021**, *42*, 129–134.
7. Huang, Y.B.; Cao, Z.S.; Lu, X.J.; Huang, J.; Liu, Q.; Dai, C.M.; Huang, H.H.; Rao, R.Z.; Wang, Y.J. Measurement of high-resolution total atmospheric transmittance and retrieval of water vapor with laser heterodyne technology. *Chin. J. Quantum Electron.* **2020**, *37*, 498–505.
8. Gong, J.R.; Liu, M.; Wang, H.X.; Yang, F.; Kang, J.-F.; Li, B.-F. Measurement and analysis of atmospheric coherence length near sea surface. *Opt. Commun. Technol.* **2018**, *13*, 44–46.
9. Ju, P.; Fan, W.H.; Gao, W.; Zhang, T.Y. Propagation characteristics of radial phase-locked discrete vector beam generated from a Gaussian Schell-Model laser array in atmospheric turbulence. *Results Phys.* **2022**, *44*, 106115. [CrossRef]
10. Li, J.M.; Sun, X.Q.; Zhang, J. Analysis of Atmospheric Influence on the Laser Energy Density of the Target. *Optoelecfronic Technol.* **2004**, *3*, 181–183+188.
11. Rao, R.Z. Strehl Ratios and Sharpness of Collimated Laser Beam in a Turbulent Atmosphere. *Chin. J. Lasers* **2005**, *32*, 53–58.
12. Jabczyński, J.K.; Gontar, P. Impact of atmospheric turbulence on coherent beam combining for laser weapon systems. *Def. Technol.* **2021**, *17*, 1160–1167. [CrossRef]
13. Gebhardt, F.G. Atmospheric effects modeling for high-energy laser systems. In Proceedings of the SPIE—The International Society for Optical Engineering, Friedrichshafen, Germany, 5–9 September 1995; Volume 2502, pp. 101–110.
14. Song, X.K.; Hong, D.; Wang, Y.; Liu, H.R.; Liu, L.F.; Li, Y.J. The Effect of Laser Energy and Target-Substrate Distance on the Quality of CeO2 Seed Layer Deposited by PLD. *J. Supercond. Nov. Magn.* **2011**, *24*, 1659–1663.
15. Jumper, G.Y.; Roadcap, J.R.; Adair, S.C.; Seeley, G.P.; Tasknumber, S. Atmospheric Considerations in Engagement-Level Simulations of Tactical High-Energy Laser Systems. *J. Dir. Energy* **2005**, *1*, 183–201.
16. Li, Y.N.; Tang, L.T.; Xie, X.Y.; Yin, F.; Shen, L.J. Measuring far-field instantaneous facula intensity space-time distribution of solid-state laser. *Infrared Lasers Eng.* **2016**, *45*, 817002.
17. Hou, L.B.; Zou, Y.G.; Ma, X.H.; Wang, L.; Zhang, H.; Yang, J.J.; Wang, D.; Hai, Y.N. Study on far-field distribution of high power semi-conductor laser beam. In Proceedings of the 2015 International Conference on Optoelectronics and Microelectronics (ICOM), Changchun, China, 16–18 July 2015.
18. Kodama, R. High energy density sate, material and device with high power lasers. In Proceedings of the 2009 Conference on Lasers and Electro Optics and The Pacific Rim Conference on Lasers and Electro-Optics, Shanghai, China, 30 August 2009.
19. Smith, P.A.; Veldhuizen, D.A.V.; Polhamus, G.D. High-energy laser systems: Analytical risk assessment and probablility density functions. In Proceedings of the BiOS 2001 The International Symposium on Biomedical Optics, San Jose, CA, USA, 17 May 2001.

20. Liu, J.M.; Wu, D.; Hu, X.H.; Liu, S.M.; Wu, H.C.; Hai, R.; Li, C.; Ding, H.B. Study of spectral intensity of the laser ablated tungsten plasma and ablation mass at various laser spot sizes and laser fluence in vacuum environment. *Spectrochim. Acta Part B At. Spectrosc.* **2023**, *199*, 106569. [CrossRef]
21. Link, D.J.; John, R.S. Simulation and modeling of high energy laser systems. In Proceedings of the Laser Technologies for Defense and Security SAIC, Orlando, FL, USA, 10 September 2004.
22. Yang, S.; Xu, K.; Zhang, Z.Y.; Wu, Y.C.; Dai, X.R.; Zhu, H.; Liu, Y. Effect of laser spot overlap on the mechanical properties and corrosion resistance of laser-assisted electrodeposited Ni-based coatings. *Mater. Chem. Phys.* **2022**, *292*, 126830. [CrossRef]
23. Yuan, Y.S. Research on Mean Irradiance Profile of a Gaussian Beam under Pointing-tracking Error. Master's Thesis, University of Electronic Science and Technology, Sichuan, China, 2019.
24. Hong, Y.U.; Wen, M.H. Error analysis of ATP simulation based on Bergeron model. *Relay* **2007**, *35*, 14–17.
25. Zhao, D.F.; Dai, Y.P.; Yin, X.H. Error Analysis for the Optical System of Target Area on High Power Laser Facility. *Chin. J. Laser* **2004**, *31*, 1425–1428.
26. Liu, X.L.; Zhang, G.X.; Li, X.H. Optical error analysis in the laser tracking measure system. *Opt. Technol.* **2004**, *30*, 245–250.
27. Wan, H.; Cao, H.; Luan, S.-Y. Investigation of thermal damage in continuous wave laser-induced nanowelding. *Opt. Laser Technol.* **2023**, *161*, 109143. [CrossRef]
28. Liu, K.; Liu, B.L.; Zhou, H.G. The damage effect of space-based laser on GEO satellites. *Spacecr. Environ. Eng.* **2022**, *39*, 545–551.
29. Wang, X.M.; Wang, J.; Guo, Z. Mathematical Model for Dynamic Damage Probability of the CW High-energy Laser Devices. *Fire Control Command Control* **2016**, *41*, 55–59.
30. Perram, G.P.; Cusumano, S.J.; Hengehold, R.L.; Fiorino, S.T. *Introduction to Laser Weapon Systems*; Directed Energy Professional Society: Albuquerque, NM, USA, 2010.
31. Tian, F.Q.; Li, K.Y. *Shipboard Laser Weapon Tracking and Aiming Control*; National Defense Industry Press: Beijing, China, 2015.